(Received 10 September 2024, Accepted 11 October 2024, Scheduled 21 October 2024)

Nonlinear Modelling of K-Band GaN Power Amplifier

Zhanglei Song[1], Xin Cheng[1], Fayu Wan[1,*], Xiaohe Chen[2], Eugene Sinkevich[3], Vladimir Mordachev[3], and Blaise Ravelo[1]

[1]*Nanjing University of Information Science & Technology, Nanjing 210044, China*
[2]*China University of Petroleum, Beijing 100100, China*
[3]*Belarusian State University of Informatics and Radioelectronics, Minsk 220013, Belarus*

ABSTRACT: An innovative nonlinear (NL) modelling of K-band power amplifier (KPA) designed and fabricated in Gallium Nitride (GaN) technology operating at frequency $f_0 = 24$ GHz is investigated in this paper. Two KPA prototypes are characterized by single- and double-frequency tests (SFT and DFT). Then, fitting memory NL model from SFT established for input-output power (P_{in}-P_{out}) characteristic @ f_0 enables the confirmation of KPA performance. Accordingly, the KPA presents 27.8 dB gain when P_{in} increases from -5 dBm to 20 dBm, 40.8 dBm saturation output power, and 38.6% saturation power added efficiency (PAE). Moreover, the DFT with $f_1 = 23.995$ GHz and $f_2 = 24.005$ GHz enables the assess to the third-order intermodulation distortion (IMD3) which is assessed from 10.4 dBc to 35 dBc. The KPA critical IMD3 is identified with the P_{out} variation range from 16.35 dBm to 36.35 dBm. The developed NL model is useful in the future for the electromagnetic interference prediction of multi-carried front-end transceiver communication system due to NL distortion signal.

1. INTRODUCTION

To meet the public demand, communication circuit and system design evolves toward the 6G technology [1, 2]. Behind the performance enhancement, transceiver (TxRx) is developed under challenging requirements [3–5]. Electromagnetic interference (EMI) challenges are currently hot topics of 6G TxRx system development [3, 4]. Among the challenging problems, innovative techniques are needed to overcome EMI induced by active circuit nonlinear (NL) effects especially at higher multi-carried frequency for example in the K-band [6, 7]. Therefore, NL analysis attracts particularly circuit design research engineers' attention. For example, relevant methods of modelling and simulation of EMI prediction due to the NL active circuits constituting the front-end system were investigated [8]. The unintentional NL effects are essentially related to RF and microwave power amplifiers (PAs) constituting the transmitter (Tx) front-end. The PA NL effect creates harmonic distortion causing intermodulation (IM) signals and unwanted transceiver EMIs [9–18]. The high-frequency (HF) harmonic distortion degrading the modulated signals cannot be neglected [8, 9]. Therefore, the NL analysis [11, 12] and modelling of active circuits as PA attracts the design research engineers [13–15].

So far, different methods of active device NL analysis as multi-parameter [16], state-space approach [17], harmonic balance [18], and Volterra series representation [19, 20] have been developed. Nevertheless, due to the circuit test and modelling difficulty, most of research works available in the literature [21–29] on RF and microwave circuit NL effect were carried out under 10-GHz. For this reason, the circuit modelling must be completed by NL experimental characterization [21–26]. Nonetheless, to analyze the unintentional EMI issues degrading the communication signals, most of NL characterizations are based on experimental methods to assess the third order IM (IM3) from two-tone carrier input signal [22–29]. But the double frequency NL method does not enable the prediction of the 5G or 6G front-end TxRx EMI operating with multi-carrier frequency interference. Meanwhile, today, more relevant methods enabling the characterization of IMs constitute the breakthrough of RF and microwave design and research engineers.

As a logic solution, multi-tone signal test method is expected to study the IMs degrading the 6G TxRx system performance [1–3]. However, few studies were available in the literature on $f_0 = 24$-GHz NL modelling and IM3 distortion (IMD3). For this reason, the present research work develops an innovative NL model of K-band PA (KPA) as a device under test (DUT) at frequency f_0.

2. NL TEST SETUP AND ANALYTICAL MODELLING

The design of KPA and NL test setup is examined in this section.

2.1. PoC Specifications

Two KPAs under study dedicated to operating around frequency f_0 were designed and fabricated. The synoptic diagram and photos of GaN KPA DUTs are represented in Fig. 1. It acts as a broadband KPA designed with a K-connector RF input interface and WR28 waveguide RF output interface. The KPA has 25-dB typical small signal gain, 20-dB typical power gain, 40-dBm

* Corresponding author: Fayu Wan (fayu.wan@nuist.edu.cn).

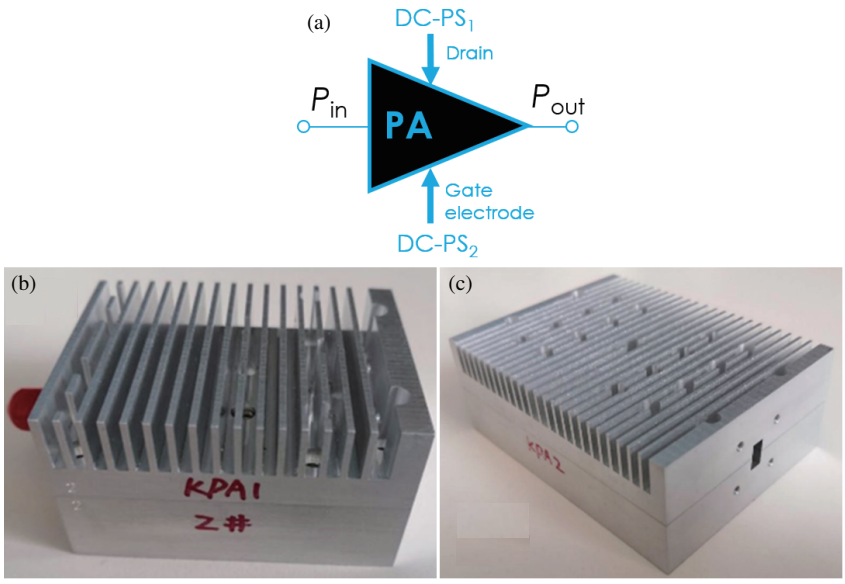

FIGURE 1. (a) PA synoptic diagram. (b) KPA1 and (c) KPA2 prototype photos.

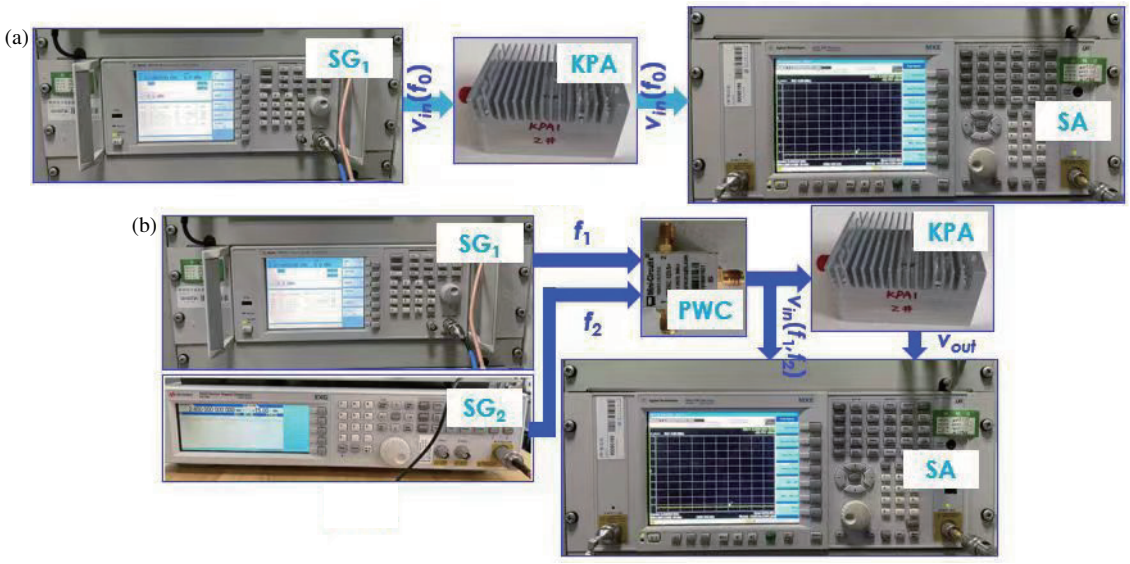

FIGURE 2. KPA (a) SFT and (b) DFT synoptic diagrams.

saturated output power, and 25-dBm maximum allowable input power.

In normal operation, PA was fed by two DC power supplies (PSs) referenced by Agilent E3632A and Agilent E3648A through its gate and drain connection ports. As illustrated by Fig. 2(a), the SFT NL test synoptic diagram with input voltage v_{in} excites the KPA to generate output v_{out}, whereas the synoptic diagram of the developed NL test bench of DFT is depicted in Fig. 2(b). The DFT input signal is restituted from harmonic components obtained by combining the outputs $v_1(f_1)$ from SG_1 and $v_2(f_2)$ from SG_2 which represent the utilized signal generators (SGs). In order to control the parameters of $v_1(f_1)$ and $v_2(f_2)$ constituting input $v_{in}(f_1, f_2)$, these two different SGs are needed. The SFT can be understood from the diagram by removing one of SGs and without power combiner.

The employed test instruments in the experimental setup are specified as SG_1 to provide input signal v_1 referenced as Agilent E8267D, SG_2 to provide input signal v_2 referenced as SMB 100A, the spectrum analyzer (SA) referenced as Agilent E4447A to measure and monitor the spectrum of v_{out}, an attenuator with 20-dB nominal value referenced 2.92TS20-20-40 to protect the SA against the damage risk from tested signal high-power and several coaxial lines gathered with adapters to connect all instruments and the DUT. The analytical approach on the PA NL modelling is expressed in the next subsection.

2.2. P_{in}-P_{out} Characteristic Modelling

From the SFT $P_{in}-P_{out}$ characteristic data and the corresponding PA gain $G = P_{out}/P_{in}$, the traditional polynomial NL model incorporating memory effects can be established. The fitting model representing the PA dynamic nonlinearity is expressed as:

$$z(n) = \sum_{i=0}^{p}\sum_{j=0}^{q} a_{ij}x(n-j)|x(n-j)|^i \tag{1}$$

where $x(n)$ and $z(n)$ are the KPA input and output signal voltages, and p and q are the polynomial order and memory depth. Substituting the input-output data into the memory polynomial model, one gets a system of equations with unknowns a_{ij} and indexes $0 \leq i \leq p$ and $0 \leq j \leq q$:

$$X \cdot a = z \tag{2}$$

with X being a matrix formed by input signals, a a column vector composed of a_{ij}, and z a column vector formed by output signals. The following linear equation system is derived from relation (2):

$$X^T \cdot X \cdot A = X^T \cdot z \tag{3}$$

After calculating the least square solution, it yields polynomial coefficients a_{ij} with $0 \leq i \leq p$ and $0 \leq j \leq q$. After the SFT result modelling, the IMD3 from the DFT is described in the following subsection.

2.3. Expression of PA Model NL Coefficients

By assuming DFT input with frequencies $f_1 < f_2$ and $\Delta f = f_2 - f_1 \ll f_0$, the harmonic component $v_{m=1,2}$ of v_{in} with amplitude $A_{m=1,2}$ and angular frequency $\omega_m = 2\pi f_m$ is expressed as:

$$v_m(t) = A_m \cos(\omega_m t). \tag{4}$$

Hence, the input signal generated from the DFT experimental setup shown in Fig. 1(b) can be expressed as $v_{in} = v_1 + v_2$. If the network is memoryless, by taking real coefficients $k_{m=1,2,3}$, the corresponding output can be expressed as a t-time dependent power series:

$$v_{out}(t) = \sum_{m=1}^{3} k_m v_{in}^m(t) \tag{5}$$

It is noteworthy that the present KPA study is limited to weak NL case ($k_m = 0$ if $m > 3$). According to the standard, most of TxRx IMD3 considered should not exceed 40 dBc. The NL coefficients are determined by linearization of SFT input $v_{in}(t) = A\cos(\omega_0 t)$ with $\omega_0 = 2\pi f_0$ as a function of range in $A = amplitude(v_{in})$ at frequencies $f = \{0, f_0\}$. For example, we assume that the fundamental component of output signal is expressed by $v_{out}(t) \approx A_{out}\cos(\omega_0 t)$ having $A_{out} = amplitude(v_{out})$. For the weak NL case, the small signal input amplitude is delimited by $0 < A \leq 0.1$ V. By means of analytical exploration of Equation (5), the NL coefficient k_1 can be estimated from output spectrum:

$$k_1 = A_{out,small}(f = f_0)/A_{small}(f = f_0). \tag{6}$$

After linearization of $v_{out}(t)$ with respect to single-tone input $v_{in}(t)$ with weak signal input amplitude belonging to the range $0.1\,\text{V} < A \leq 0.3\,\text{V}$, the NL coefficients k_2 and k_3 estimated from output spectrum at frequencies $f = \{0, f_0\}$ can be determined from equations:

$$\begin{cases} k_2 = 2A_o(f=0)/A^2(f=0) \\ k_3 = \dfrac{4[A_o(f=f_0) - k_1 A(f=f_0)]}{3A^3(f=f_0)} \end{cases}. \tag{7}$$

The DFT NL test consists in measuring the IM3 of combined fundamental frequency components $f_{m=1,2}$. If the considered test circuit is memoryless, the corresponding NL model can be expressed as represented in Equation (5) by taking real coefficients $k_{m=1,2,3}$. Through the established polynomial model, a series of frequency combination components generated by the output can be intuitively analyzed, and the interference components in the output response of the power amplifier can be obtained. Based on the proposed NL model, the KPA output for different harmonic amplitudes is approximated as discussed in the next section which is dedicated to the experimental result examination.

3. DISCUSSION ON KPA EXPERIMENTATION AND NL CHARACTERISTIC MODELLING RESULTS

The present section describes the obtained NL experimental and empirical modelling results of KPA based on the measured input and output powers.

3.1. Fitting Memorial Polynomial Modelling Results

During the SFT operating at frequency f_0, the input power P_{in} was gradually increasing from $P_{in,\text{min}} = 0$ dBm to $P_{in,\text{max}} = 20$ dBm with 1 dBm step. Fig. 3(a) and Fig. 3(b) show the KPAs gain and efficiency from the SFT versus P_{out}, respectively. The efficiency corresponding to measured P_{in} and P_{out} is calculated from equation $\xi(\%) = 100(P_{out} - P_{in})/P_{DC}$ by taking P_{DC} as the DC power supply.

Moreover, measured values of P_{out}, gain, and efficiency at particular values of P_{in} are summarized in Table 1. As results of experimental characterization, at f_0, KPA1 has $G = 27.8$ dB, saturation power $P_{sat} = 40.821$ dBm and $\xi = 38.31\%$. Then, KPA2 presents $G = 26.6$ dB, $P_{sat} = 40.971$ dBm and $\xi = 39.97\%$.

TABLE 1. KPA prototypes NL characteristics from SFT.

P_{in} (dBm)	KPA	0	5	10	20
P_{out} (dBm)	KPA1	27.769	32.892	36.928	40.821
Gain (dB)		27.419	27.542	26.578	21.471
ξ (%)		2.72	8.89	20.44	38.31
P_{out} (dBm)	KPA2	26.137	32.007	36.545	40.981
Gain (dB)		25.787	26.657	26.195	21.611
ξ (%)		1.86	7.25	18.71	39.97

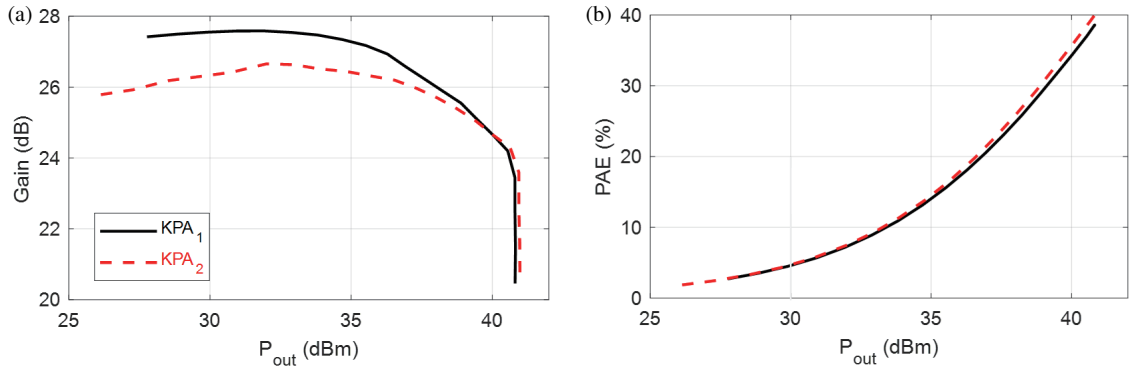

FIGURE 3. KPA1 and KPA2 (a) gain and (b) PAE vs $Pout$.

TABLE 2. KPA P_{in}-P_{out} characteristic coefficients of the memory polynomial model.

j/i	1	2	3	4	5	6	7
1	1.935	13.282	-	-	-	-	-
2	−0.855	26.196	−6.514	-	-	-	-
3	−0.756	25.406	−5.510	−0.310	-	-	-
4	−0.474	22.183	1.762	−5.585	1.182	-	-
5	−0.450	21.826	2.983	−7.103	1.954	−0.137	-
6	−0.058	14.547	37.437	−71.079	56.442	−21.549	3.146

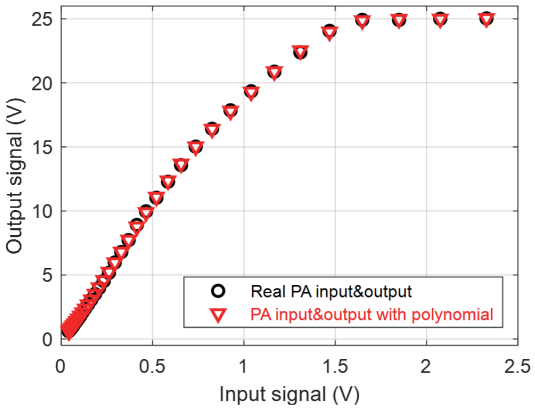

FIGURE 4. Comparison of fitted model and measured KPA P_{in}-P_{out} characteristic.

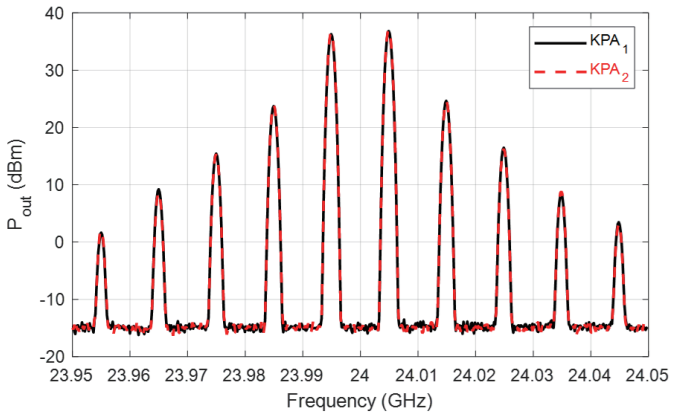

FIGURE 5. KPA1 and KPA2 output spectra with $P_{in} = 15$ dBm.

3.2. KPA Fitting Memorial Polynomial Modelling

According to Ohm's law, the harmonic signal amplitude equals the square root of the signal power multiplied by the characteristic impedance which is 50-Ω. When the polynomial order is $p = 5$ and the memory depth $q = 6$, by converting the powers in dBm into voltage in V, the coefficients of the memory polynomial are computed using MATLAB. The obtained coefficients are addressed in Table 2. Fig. 4 shows the comparison between the MPA P_{in}-P_{out} characteristic obtained through polynomial fitting indicated in Table 2 with the aforementioned coefficients and the measured P_{in}-P_{out} characteristic.

After the fitting modelling, the KPA IMD3 from DFT results is analyzed. From Fig. 4, the fitted P_{in}-P_{out} characteristic aligns closely with the measured ones.

Due to the memory effect represented by the polynomial model, the first six points cannot be accurately plotted when the memory depth is set to $q = 6$.

3.3. KPA IMD3 Analysis from DFT Results

The present subsection focuses on the analysis of IM3s $2f_1 - f_2$ and $2f_2 - f_1$ when the input fundamentals are fixed to $f_1 = 23.995$ GHz and $f_2 = 24.005$ GHz with same amplitudes $A_1 =$

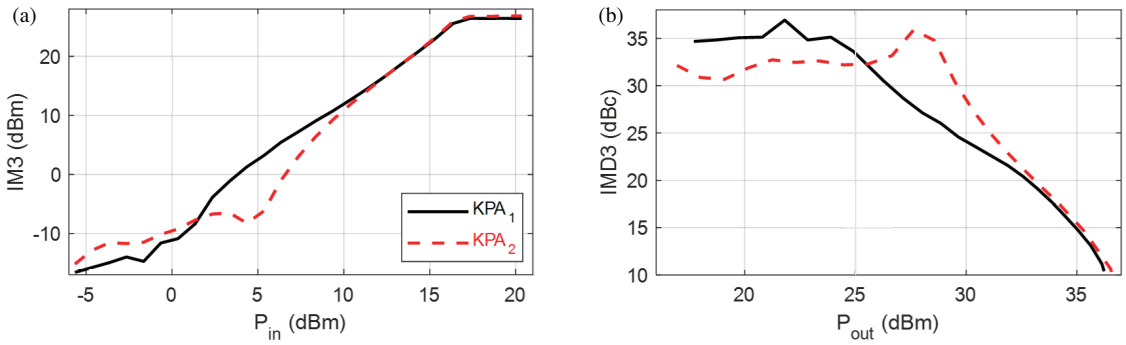

FIGURE 6. KPA1 and KPA2 (a) IM_3 vs P_{in} and (b) IMD_3 vs P_{out}.

TABLE 3. Comparison of PA IMD3 detection methods.

Ref.	Method	Complexity	Cost
[30]	SFT and DFT	-	-
[31]	DFT and MFT	-	-
[32]	DFT and LTE Signal Test	Complex	-
[33]	Automatic DFT	-	-
This work	Automatic SFT and DFT	Simple	5 min

A_2 from DFT introduced in Fig. 2(b). The IM3 was empirically evaluated by gradually increasing P_{in} from $P_{in,\min} = -5$ dBm to $P_{in,\max} = 20$ dBm. The mathematical variation law governing the KPAs IM3 with respect to P_{in} is studied. One recalls that the IMD3 is calculated by equation IMD3 $= P_{in} -$ IM3. Then, the IM3 component power is recorded and drawn. By increasing P_{in}, one observes whether IM3s appear near the spectrum of P_{out} displayed in Fig. 5 spanned from 23.98 GHz to 24.02 GHz. After the observation and analysis of IM3s, the signal power is recorded synchronously, the input and IM3 characteristic curve of the KPA is plotted. Then, the KPA IMD3 was calculated by adjusting the SG MOD mode to have the dual-tone signal. During the DFT, the SG output was gradually increased from -5 dBm to 20 dBm by considering the power step 1 dBm interval until the SA is able to plot the expected IM3.

In practice, the SA marker was handled to record the test signal having spectrum constituted by components $2f_1 - f_2 = 23.985$ GHz, $f_1 = 23.995$ GHz, $f_2 = 24.005$ GHz and $2f_2 - f_1 = 24.015$ GHz. It corresponds to the spectrum power showing the IM3. It is worth to note that the attenuation and loss can be assessed from the output signal of the KPA DUTs. Therefore, we have the KPAs IM3 test data which are displayed in Fig. 6. In addition, the KPA IMD3s were calculated, implying the P_{in} vs IM3 and P_{out} vs IMD3 characteristic diagram drawn as shown in Fig. 6(a) and Fig. 6(b), respectively.

The following remark can be underlined:

- The two IMD3s are equal in theory, but in practice they can only be close due to factors such as signal source and attenuation.
- From the obtained IM3 diagrams of Fig. 6(b), one finds that the DFT induces small experimental error and guarantees considerable accuracy.
- As P_{in} increases gradually, the KPAs enters the NL region. Based on the behavioral plot of Fig. 6(a), the IM3 increase rate is greater than the fundamental component one.
- Moreover, as P_{in} increases gradually, IMD3 gradually decreases when $P_{out} \approx 32.6$ dBm. Therefore, IMD3 of KPA1 and KPA2 is greater than 20.912 dBc. Such a measured value of DUT IMD3 meets industrial design requirements and corresponds to weak NL distortion.

3.4. Advantages of Developed NL Characterization

The developed NL test and model can be applied to any microwave active circuits with certain benefits. Doing this, the comparison of NL technique performances is addressed in the present subsection.

Table 3 summarizes the comparison of the achieved NL performances in terms of IMD3 detection ability with the developed test technique performed study with the existing ones in the literature [30–33].

Moreover, Table 4 indicates the developed SFT and DFT performance characteristics performances and the existing ones available in the literature [34–37] in terms of PA NL specifications. The developed NL technique not only is susceptible to operate in mm-wave range but also presents benefits in terms of test setup automatization, simplicity, and handling time.

In addition, the proposed NL technique testability was verified with good performance KPAs P_{sat} and *Gain*. The per-

TABLE 4. Comparison with state-of-the-art mm-wave power amplifiers.

Ref.	Freq./GHz	Sat.P_{out}/dBm	Sat.Gain/dB	Sat.Efficiency/%	Sat. |IMD3|/dBc
[34]	25–26.5	28.9–30	5.2–6.5	29–40	-
[35]	24	15.7	17.5	30.4	-
[36]	24–29	30–31.3	-	27.6–38.9	-
[37]	24–29.5	19.2–21.3	13–15.9	23.2–28.4	-
This work	24	40.981	26.657	40.96	35.887

formance comparison enables promising potential applications of the SFT and DFT for EMI characterization of mm-wave Tx and Rx system in the future especially by assessing the NL effect influence.

4. CONCLUSION

A simple and flexible NL modelling of microwave active devices is studied. The feasibility test was verified with a proof of concept represented by two different KPAs designed and implemented in GaN technology. The methodology of SFT and DFT technique is explained.

After brief design and SFT test method description, the experimentation of KPA proof of concept (PoC) is described by considering operating frequency fixed to f_0. Then, fitting model of Pin-Pout characteristic is developed. A very good correlation between the NL performances of the two different KPA prototypes is obtained. Moreover, the influence of the KPA1 NL characteristic on the communication system is studied via DFT by assessing the IMD3.

In the future, the research work result is helpful for the EMI analysis of multicarrier front-end communication system due to the undesirable NL implying transmission signal distortion.

ACKNOWLEDGEMENT

This research work is supported by the National Key Research and Development Program of China (2022YFE0122700).

REFERENCES

[1] Saad, W., M. Bennis, and M. Chen, "A vision of 6G wireless systems: Applications, trends, technologies, and open research problems," *IEEE Network*, Vol. 34, No. 3, 134–142, May/Jun. 2020.

[2] Yaklaf, S. K. A., K. S. Tarmissi, and N. A. A. Shashoa, "6G mobile communications systems: Requirements, specifications, challenges, applications, and technologies," in *2021 IEEE 1st International Maghreb Meeting of the Conference on Sciences and Techniques of Automatic Control and Computer Engineering MI-STA*, 679–683, Tripoli, Libya, 2021.

[3] Wiklundh, K. and P. Stenumgaard, "EMC challenges with 6G," in *2022 International Symposium on Electromagnetic Compatibility — EMC Europe*, 19–24, Gothenburg, Sweden, 2022.

[4] Wiklundh, K. and P. Stenumgaard, "EMC challenges for the era of massive internet of things," *IEEE Electromagnetic Compatibility Magazine*, Vol. 8, No. 2, 65–74, Jul. 2019.

[5] Miranda, J., J. Cabral, B. Ravelo, S. Wagner, C. F. Pedersen, M. Memon, and M. Mathiesen, "Radiated EMC immunity investigation of common recognition identification platform for medical applications," *The European Physical Journal Applied Physics*, Vol. 69, No. 1, 11002, Jan. 2015.

[6] Pareschi, F., R. Rovatti, and G. Setti, "EMI reduction via spread spectrum in DC/DC converters: State of the art, optimization, and tradeoffs," *IEEE Access*, Vol. 3, 2857–2874, 2015.

[7] Mordachev, V., E. Sinkevich, Y. Yatskevich, A. Krachko, P. Zaharov, and X. Ma, "Simulation of nonlinear interference in aircraft systems operating in complex electromagnetic environment created by land-based and air-based wireless systems," in *2017 International Symposium on Electromagnetic Compatibility — EMC EUROPE*, 1–6, Angers, France, 2017.

[8] Fiori, F. L. and P. S. Crovetti, "Prediction of high-power EMI effects in CMOS operational amplifiers," *IEEE Transactions on Electromagnetic Compatibility*, Vol. 48, No. 1, 153–160, Feb. 2006.

[9] Harasis, S. K., M. E. Haque, A. Chowdhury, and Y. Sozer, "SiC based interleaved vsi fed transverse flux machine drive for high efficiency, low EMI noise and high power density applications," in *2020 IEEE Energy Conversion Congress and Exposition (ECCE)*, 4943–4948, Detroit, MI, USA, 2020.

[10] Fan, Y., Y. Guo, and L. Duan, "A wide-band GaN power amplifier with negative feedback," in *2023 IEEE 6th International Conference on Computer and Communication Engineering Technology (CCET)*, 239–243, Beijing, China, 2023.

[11] Abuelma'atti, M. T., "Analysis of the effect of radio frequency interference on the DC performance of bipolar operational amplifiers," *IEEE Transactions on Electromagnetic Compatibility*, Vol. 45, No. 2, 453–458, May 2003.

[12] Shi, G., "Symbolic distortion analysis of multistage amplifiers," *IEEE Transactions on Circuits and Systems I: Regular Papers*, Vol. 66, No. 1, 369–382, 2019.

[13] Miao, Y. and Y. Zhang, "Distortion modeling of feedback two-stage amplifier compensated with miller capacitor and nulling resistor," *IEEE Transactions on Circuits and Systems I: Regular Papers*, Vol. 59, No. 1, 93–105, 2012.

[14] Fiori, F., "A new nonlinear model of EMI-induced distortion phenomena in feedback CMOS operational amplifiers," *IEEE Transactions on Electromagnetic Compatibility*, Vol. 44, No. 4, 495–502, Nov. 2002.

[15] Li, X., C. Liu, and F. Li, "TD-SCDMA: Spectrum modeling, experimental verification of power amplifier nonlinearity," *Chinese Journal of Electronics*, Vol. 22, No. 3, 631–633, 2013.

[16] Skorokhod, Y., D. Sorokin, and S. Volskiy, "Analysis of the influence of error amplifier factors on total harmonic distortion of converter input current," in *2021 8th International Conference on Electrical and Electronics Engineering (ICEEE)*, 174–178,

Antalya, Turkey, 2021.

[17] Lin, Q., C. Lu, H.-F. Wu, and D.-H. Hu, "A high efficiency GaN PA based on the harmonic control," in *2022 International Conference on Microwave and Millimeter Wave Technology (ICMMT)*, 01–03, Harbin, China, 2022.

[18] Sandberg, I. W. and G. J. J. V. Zyl, "Harmonic balance and almost periodic inputs," in *2002 IEEE International Symposium on Circuits and Systems. Proceedings (Cat. No.02CH37353)*, 637–640, Phoenix-Scottsdale, AZ, USA, 2002.

[19] Mu, S., Z. Wu, G. Liu, Z. Chen, and W. Yu, "Design and research of a nonlinear distortion three-stage coupling amplifier," in *2021 IEEE Asia-Pacific Conference on Image Processing, Electronics and Computers (IPEC)*, 780–786, Dalian, China, 2021.

[20] Sweeney, C., D. Y. C. Lie, J. Mayeda, and J. Lopez, "5G FR2-band PA performance degradation in 40-nm GaN HEMTs with potential design solutions," in *2024 International Conference on Consumer Electronics — Taiwan (ICCE-Taiwan)*, 411–412, Taichung, Taiwan, 2024.

[21] Fu, K., C. L. Law, and T. T. Thein, "Test bed for power amplifier behavioral characterization and modelling," *Measurement*, Vol. 46, No. 8, 2735–2745, 2013.

[22] Mordachev, V. and E. Sinkevich, "Experimental analysis of radio receiver susceptibility to out-of-band interference by means of double-frequency test system," in *10th International Symposium on Electromagnetic Compatibility*, 405–411, York, UK, 2011.

[23] Sinkevich, E. and V. Mordachev, "Investigation of the transmitter susceptibility to reverse intermodulation by the use of double-frequency diagrams," in *2015 IEEE International Symposium on Electromagnetic Compatibility (EMC)*, 1159–1164, Dresden, Germany, 2015.

[24] Panigrahi, S. R. and D. Rönnow, "Evaluating nonlinear distortion of single and dual channel excitation of an amplifier at 24 GHz," *Microwave and Optical Technology Letters*, Vol. 63, No. 9, 2315–2319, 2021.

[25] Alizadeh, M., D. Rönnow, and P. Händel, "Characterization of Volterra kernels for RF power amplifiers using a two-tone signal and a large-signal," in *2018 International Conference on Communications (COMM)*, 351–356, Bucharest, Romania, 2018.

[26] Mordachev, V., E. Sinkevich, and D. Petrachkov, "Representation and analysis of radio receivers' susceptibility and nonlinearity by the use of 3D double-frequency characteristics," in *2014 International Symposium on Electromagnetic Compatibility, Tokyo*, 689–692, Tokyo, Japan, 2014.

[27] Yang, G., H. Li, W. Qiao, C. Jiang, Q. Liu, G. Wang, and F. Liu, "Digital predistortion based on sample selection with memory effect," *International Journal of RF and Microwave Computer-Aided Engineering*, Vol. 32, No. 2, e22976, 2022.

[28] Huang, C., J. Wu, and L. Shi, "On the use of multi-tone for the estimation and measurement of noise power ratio in third-order nonlinear system," *Chinese Journal of Electronics*, Vol. 19, No. 4, 763–768, 2010.

[29] Su, J., J. Cai, X. Zheng, and L. Sun, "A fast two-tone active load-pull algorithm for assessing the non-linearity of RF devices," *Chinese Journal of Electronics*, Vol. 31, No. 1, 25–32, 2022.

[30] Cai, Q., W. Che, K. Ma, and M. Zhang, "A simplified transistor-based analog predistorter for a GaN power amplifier," *IEEE Transactions on Circuits and Systems II: Express Briefs*, Vol. 65, No. 3, 326–330, Mar. 2018.

[31] Qian, H. and J. Silva-Martinez, "Multitone ACLR and its applications to linear PA design," *IEEE Transactions on Circuits and Systems II: Express Briefs*, Vol. 64, No. 10, 1177–1181, Oct. 2017.

[32] Latha, Y. M. A. and K. Rawat, "Design of ultra-wideband power amplifier based on extended resistive continuous class B/J mode," *IEEE Transactions on Circuits and Systems II: Express Briefs*, Vol. 69, No. 2, 419–423, Feb. 2022.

[33] Mordachev, V. I., "Automated double-frequency testing technique for mapping receive interference responses," *IEEE Transactions on Electromagnetic Compatibility*, Vol. 42, No. 2, 213–225, May 2000.

[34] Chen, P., R.-J. Liu, L. Yu, Z. Zhao, X.-W. Zhu, D. Hou, J. Chen, C. Yu, and W. Hong, "An optimization method for load modulation trajectories in a millimeter-wave GaN MMIC Doherty power amplifier design," *IEEE Transactions on Circuits and Systems II: Express Briefs*, Vol. 71, No. 1, 141–145, Jan. 2024.

[35] Li, J., B. Sun, J. Huang, L. Wu, H. Chang, R. Jia, and H. Liu, "A K-band broadband power amplifier with 15.7 dBm power and 30.4CMOS," *IEEE Transactions on Circuits and Systems II: Express Briefs*, Vol. 70, No. 4, 1321–1325, Apr. 2023.

[36] Cai, Q., H. Zhu, D. Zeng, Q. Xue, and W. Che, "A three-stage wideband GaN PA for 5G mm-wave applications," *IEEE Transactions on Circuits and Systems II: Express Briefs*, Vol. 69, No. 12, 4724–4728, Dec. 2022.

[37] Wang, D., W. Chen, X. Chen, X. Liu, F. M. Ghannouchi, and Z. Feng, "A 24-29.5 GHz voltage-combined Doherty power amplifier based on compact low-loss combiner," *IEEE Transactions on Circuits and Systems II: Express Briefs*, Vol. 68, No. 7, 2342–2346, Jul. 2021.